HHS Public Access

Author manuscript

Abdom Radiol (NY). Author manuscript; available in PMC 2022 February 27.

Published in final edited form as:

Abdom Radiol (NY). 2019 December ; 44(12): 3919–3934. doi:10.1007/s00261-019-02086-0.

What a difference a delay makes! CT urogram: a pictorial essay

Abraham Noorbakhsh[1], **Lejla Aganovic**[1,2], **Noushin Vahdat**[1,2], **Soudabeh Fazeli**[1], **Romy Chung**[1], **Fiona Cassidy**[1,2]

[1]Department of Radiology, University of California, San Diego Health, San Diego, USA

[2]Department of Radiology, Veterans Affairs San Diego Healthcare, San Diego, CA, USA

Abstract

Purpose—The aim of this pictorial essay is to demonstrate several cases where the diagnosis would have been difficult or impossible without the excretory phase image of CT urography.

Methods—A brief discussion of CT urography technique and dose reduction is followed by several cases illustrating the utility of CT urography.

Results—CT urography has become the primary imaging modality for evaluation of hematuria, as well as in the staging and surveillance of urinary tract malignancies. CT urography includes a non-contrast phase and contrast-enhanced nephrographic and excretory (delayed) phases. While the three phases add to the diagnostic ability of CT urography, it also adds potential patient radiation dose. Several techniques including automatic exposure control, iterative reconstruction algorithms, higher noise tolerance, and split-bolus have been successfully used to mitigate dose. The excretory phase is timed such that the excreted contrast opacifies the urinary collecting system and allows for greater detection of filling defects or other abnormalities. Sixteen cases illustrating the utility of excretory phase imaging are reviewed.

Conclusions—Excretory phase imaging of CT urography can be an essential tool for detecting and appropriately characterizing urinary tract malignancies, renal papillary and medullary abnormalities, CT radiolucent stones, congenital abnormalities, certain chronic inflammatory conditions, and perinephric collections.

Keywords

CT urography; Pictorial essay; Low-dose techniques

Introduction

In recent years, CT urography has become the primary imaging modality for evaluation of hematuria and has largely replaced the intravenous pyelogram [1]. Common indications for CT urography include work-up of asymptomatic hematuria, gross or microscopic, and staging or surveillance of urinary tract malignancies [2]. At the time of this writing, ACR

✉Fiona Cassidy, Fcassidyhughes@yahoo.com.

Disclosures

The authors have no disclosures to report.

Appropriateness Criteria exist for hematuria and bladder cancer that guide the appropriate use of CT urography in these settings (Table 1) [3–6]. Excretory phase imaging of CT urography can serve as a useful troubleshooting tool in patients with evidence of obstruction, trauma, or congenital abnormalities seen on initial non-contrast or single-phase contrast-enhanced CT examinations [2]. It is also indicated in post-surgical patients, particularly for delineating anatomy in patients with urinary diversions and in the early post-operative phase of partial nephrectomy where urine leak is a concern. CT urography is generally preferred over MR urography due to higher-spatial resolution, although MR urography can be used in patients with contraindications to iodinated contrast and in the pregnant patient [7].

Despite its routine use, there is currently no consensus protocol for performing CT urography. The most common protocol is a three-phase technique, which carries potential for substantial radiation exposure to the patient. In fitting with the ALARA (as low as reasonably achievable) principle, it is the duty of the radiologist to continually revisit and optimize protocols to achieve the lowest possible radiation dose while maintaining diagnostic image quality [8].

Utilization of automated exposure control (AEC) and implementation of various iterative reconstruction (IR) algorithms have both resulted in substantial dose reductions in abdominal CT imaging [9–12]. Development of a split-bolus technique combines the nephrographic and excretory phases into a single series at the expense of suboptimal contrast enhancement and lesion characterization, and is most frequently used in younger adults to further reduce dose. Additional dose reductions have come from data showing that incompletely opacified ureteral segments on an initial excretory phase scan are highly unlikely to contain malignancy and thus, do not require repeat delayed excretory phases to exclude ureteral tumors [13]. There are several single-institution retrospective studies suggesting that a single non-contrast phase CT exam may be sufficient in patients under 40 to 50 years evidenced by an exceptionally low yield of malignant causes of hematuria detected by CT urography among this younger group, and with one study citing a theoretical risk of upper urinary tract malignancy in patients under 50 at 0–1.1% [14–16].

In this pictorial essay, we will describe how to perform a low-dose, high-quality CT urogram, and will present several cases of urinary tract pathology where the diagnosis may not have been made without the excretory phase images.

CT urogram technique

The CT urogram is most commonly performed as a three-phase computed tomography technique used to evaluate the kidneys and urinary collecting system. The three phases most commonly include a non-contrast phase, a nephrographic phase scanned at 80 to 120 s delay, and an excretory phase scanned at 10–15 min delay (Fig. 1). The primary purpose of the non-contrast phase is to evaluate for calcified stones or other high-density abnormalities, and to get a baseline Hounsfield unit measurement for renal masses.

The nephrographic phase should demonstrate symmetric contrast enhancement of the renal cortex and medulla. The homogeneous enhancement of the renal parenchyma makes this

phase most sensitive for detecting renal masses. The excretory phase is timed to show contrast within the urinary collecting system and has largely replaced the fluoroscopic intravenous pyelogram. The excretory phase should demonstrate symmetric excretion with opacification of bilateral ureters. This phase is particularly sensitive for detecting filling defects in the excreted contrast column, which may indicate a mass or other abnormalities within the urinary collecting system.

The multiphase imaging of CT urography provides an opportunity for selective dose reduction in those phases that may tolerate higher levels of image noise while maintaining diagnostic confidence [17]. Radiation dose is most commonly lowered by reducing the tube current, or milliamperes (mA); however, dose reduction can also be achieved by lowering the tube potential, or kilovoltage peak (kVp). While lower tube potential is more routinely applied in pediatric imaging, it is infrequently applied in the adult population undergoing abdominal CT [18]. Unlike tube current, tube potential has a non-linear relationship on radiation dose. Compared with 80 kVp, radiation output is 1.5 times higher at 100 kVp, and 2.5 times higher at 120 kVp [19]. This reduction in dose comes at the expense of increased image noise. This can be partially compensated for by increasing mA or application of noise reduction filters, but remains a major limiting factor in larger adult patients [20, 21].

Despite these limitations, lower kVp may be advantageous in certain contrast-enhanced exams. Due to closer approximation of the X-ray beam to the K-edge of iodine, iodinated-contrast agents have increased attenuation at a lower tube potential [19]. The resulting improvement in the image contrast of iodine may outweigh the increased noise, maintaining or potentially improving conspicuity of contrast-enhanced urothelial lesions and ureteral irregularities on CT urography.

Dual-energy CT provides the potential to further reduce dose by acquiring a single excretory-phase series and generating virtual non-contrast images. However, limitations include increased noise, lower sensitivity for 1–2 mm stones, and difficulty in obtaining accurate attenuation measurements [22, 23]. While dual-energy CT has not gained widespread adoption, recent improvements in the technique to address these limitations make dual-energy applications still promising [24].

Institutional protocol and dose-reduction strategies

In patients over 40 years of age, we have created a low-dose multiphase protocol at our institution (Table 2). Patients are instructed to hydrate well on the day of the CT urogram and not to urinate for 1 h prior to the exam. Non-contrast images are obtained through the kidneys only with a standard kVp of 120, but with reduced mA. This is achieved through reducing the image quality selection parameter, which at our institution is done by increasing the fixed noise index (GE Healthcare) from 32 to 37, and using AEC. Low kVp imaging was not applied to the non-contrast phase because of the need for accurate measurement of attenuation values (Hounsfield units) to assess for lesion enhancement, and reduction in tube potential increases measured Hounsfield values of all tissues relative to scans performed at higher kVp. Nephrographic phase images are obtained through the kidneys and bladder at 90-s delay following injection of IV contrast material at 1.5 mL/kg

up to maximum of 120 mL, which is then chased by a 250-mL saline bolus. Standard fixed noise index of 32 and kVp of 120 are used for the nephrographic phase. Excretory phase images are obtained through the kidneys and bladder after a 10-min delay. Dose reduction is achieved on the excretory phase by reducing the kVp to 100 and increasing the fixed noise index from 32 to 37. The patient is rolled 360 degrees on the table just before the excretory phase is acquired to ensure homogenous contrast in the bladder.

Using this protocol, we achieved approximately 30% dose reduction compared to our previous protocol for patients over 40 years of age while still maintaining a high-quality nephrographic phase exam through the abdomen and pelvis and allowing accurate assessment of enhancement of renal lesions. The total mean effective dose of the low-dose protocol was 13.2 mSv (median, 11.8 mSv; range, 9.8–19.5 mSv).

In patients under the age of 40, we implemented a split-dose protocol. This reduces radiation dose in the younger patient by obtaining a combined nephrographic-excretory phase acquisition. The disadvantage is that it may result in more streak artifact, which can result in pseudo-enhancement of renal masses, reducing the ability to characterize renal parenchymal lesions. However, this is more acceptable in a younger patient where the incidence of malignancy and renal lesions, including cysts, is lower. The protocol involves an initial non-contrast CT through the kidneys and bladder with reduced mA—again achieved by increasing the fixed noise index to 37—to evaluate for renal stones. A half or less than half dose of intravenous contrast material is then injected (approximately 0.75 mL/kg up to a maximum of 75), chased by a saline bolus. This is followed by the administration of the remaining dose (also approximately 0.75 mL/kg) at approximately a 90-s delay. Post-contrast mages are then acquired through the bladder and kidney using the same low-dose parameters as the non-contrast phase. This allows for both nephrographic and excretory phase imaging to be obtained in a single acquisition. Using the split-bolus protocol (for patients < 40 years of age) resulted in a further mean decrease in effective dose of 18% compared to our new low-dose protocol for patients over 40. The total mean effective dose of the split-bolus protocol was 10.8 mSv (median, 10.9 mSv; range, 8.9–12.6 mSv).

Urinary tract malignancies

In our practice, the most common indication for CT urography is for evaluation of hematuria to detect urinary tract malignancies. Urinary tract malignancies can be divided into upper (renal pyelocaliceal system and ureters) and lower (bladder and urethra) tracts. Urothelial carcinoma (UC)—previously known as transitional cell carcinoma prior to the 2016 update to the WHO classification of bladder neoplasms—is the most common malignant histology affecting the urinary tract [25]. Bladder UC is the most common location, comprising 90–95% of urothelial carcinomas compared to 5–10% in the upper tract [26]. Furthermore, 17% of patients diagnosed with primary upper tract UC were found to have concomitant bladder cancer in a retrospective review [27]. Urothelial carcinoma risk factors include smoking, cyclophosphamide exposure, and occupational exposures to chemical carcinogens [26, 28]. Other urinary tract malignant histologies include squamous cell carcinoma, which is associated with chronic inflammatory processes and comprises up to 5–10% of upper tract malignancies, as well as adenocarcinoma, which comprises less than 1% [29, 30].

The excretory phase of CT urography is the ideal phase for detecting malignancies within the urinary collecting system. It is timed such that urine opacifies with contrast and allows for greater contrast separation between urine and soft-tissue density, which appear as filling defects. UC can also often be detected on nephrographic phase as an enhancing urothelial mass or urothelial thickening [13]. Non-contrast CT imaging is limited in evaluation of urinary tract malignancies due to low spatial resolution and similar densities of urine and soft-tissue masses.

Multiple cases are presented here, in which the detection of urinary tract malignancy would have been difficult without the excretory phase images. Hypoenhancing urothelial cancer in the renal pelvis or calyx can often be overlooked on nephrographic phase images (Fig. 2) but is readily identified as a filling defect on the excretory phase. The excretory phase is also invaluable in distinguishing early excretion of contrast on the nephrographic phase from an enhancing soft-tissue mass (Fig. 3) and in delineating whether a soft-tissue mass in the renal sinus arises from renal parenchyma or within the collecting system (Fig. 4).

A ureteral mass, such as UC, could also serve as a lead point in ureteroureteral intussusception, which requires excretory phase imaging to make the diagnosis (Fig. 5). Although this entity has been classically thought to be associated with benign ureteral tumors or urolithiasis, there are several case reports where urothelial carcinoma served as the lead point. Cases associated with UC were more likely to be in elder patients who were asymptomatic at the time of diagnosis and subsequently found to have smaller tumors when compared to case reports of intussusception with benign entities [31].

Renal papillary/medullary abnormalities

Medullary sponge kidney

Medullary sponge kidney, also known as renal tubular ectasia, is a congenital malformation of the medullary collecting ducts with cystic dilation seen on histology [32]. Non-contrast images may only demonstrate medullary calcifications, which look similar to non-obstructing renal calculi. Contrast excretion through these abnormal collecting ducts is thought to be delayed, and results in the characteristic “paintbrush appearance” on excretory phase imaging (Fig. 6) [33]. While patients with medullary sponge kidney are often asymptomatic and the diagnosis discovered incidentally, medullary sponge kidney has been shown to be associated with increased risk of infection, increased renal calculus formation, and hematuria [32].

Renal papillary necrosis

Renal papillary necrosis is difficult to identify on standard contrast-enhanced and non-contrast CT imaging, but shows unique imaging features on the excretory phase of CT urography. As the renal papilla undergoes coagulant necrosis, a cleft or cavity may form from the calyces into the renal papilla or medulla. On excretory phase imaging, papillary necrosis may be detected from contrast-opacified urine filling the cleft or cavity, or by contrast surrounding the sloughed necrotic tissue. Renal papillary necrosis has a wide differential of etiologies, including pyelonephritis, urinary collecting system obstruction,

sickle cell disease, tuberculosis, cirrhosis, analgesic or alcohol abuse, renal vein thrombosis, diabetes mellitus, or systemic vasculitides [34]. Other imaging findings may be relevant to narrowing the differential. A case with the classic “golf ball on tee” sign is described below (Fig. 7), in which contrast opacifies into a central cavity—the golf ball—formed as a result of papillary necrosis [35].

Urinomas and perinephric fluid collections

Distinguishing urinomas from other types of perinephric fluid collections is a distinct advantage of CT urography. Perinephric fluid collections may contain simple fluid, blood, pus, or urine and could represent post-operative seroma, perinephric hematoma, perinephric abscess, or urinoma, respectively. Non-contrast and nephrographic phase imaging are generally not helpful in distinguishing between these types of perinephric fluid collections as they all demonstrate relatively similar densities on CT. Excretory phase imaging is timed to capture contrast when it opacifies the urine. Thus, the presence of contrast outside the collecting system and within the fluid collection confirms the diagnosis of urinoma. Urinomas may be post-traumatic, post-surgical/iatrogenic, or post-obstructive in etiology. Two cases of urinomas are described to demonstrate the utility of CT urography in identifying the etiology of a post-surgical fluid collection (Fig. 8), as well as a post-obstructive fomiceal rupture (Fig. 9), which is most commonly caused by distal obstructing ureteral calculi [36, 37].

CT radiolucent stones

Over 99% of renal calculi are radiodense on CT and easily detected; however, there are rare compositions of renal calculi that are indistinguishable from urine attenuation on CT [38]. Excretory phase imaging may detect the CT lucent stone as either complete obstruction with lack of distal ureter contrast opacification, or a filling defect within the excreted contrast column (Fig. 10) [39]. Note that uric acid and xan-thene stones are classically referred to as radiolucent stones given their lucent appearance on conventional radiographs, but are easily detected by CT and are not included in this section on the CT lucent stone. Two classic examples of stones that are radiolucent on CT are matrix stones and drug-induced stones from protease inhibitors, such as indinavir. The incidence of indinavir-related urolithiasis is reported to range from 3% up to 22% in HIV patients taking indinavir [40]. Matrix calculi are composed predominantly of mucoproteins and mucopolysaccharides, containing approximately two-thirds protein and one-third carbohydrate by weight and with minimal to no mineralization. Although no clear age predilection is evident, prior case reports and series suggest there may be an association with female gender, history of recurrent renal calculus formation, prior surgical intervention for renal calculi, and chronic urinary tract infection (UTI)—particularly with *Proteus* species and *E. coli*. These case series have described imaging findings of matrix stones as radiolucent filling defects on intravenous pyelography or soft-tissue densities in the renal pelvis, sometimes with scattered or rim calcification [41, 42].

Congenital abnormalities

CT urography is particularly useful in delineating the urinary collecting system anatomy, and thus naturally lends itself to better characterizing congenital abnormalities.

Ureterocele

Ureteroceles represent congenital dilatation of the distal-most portion of the ureter and may herniate into the bladder. They are thought to arise from obstruction of the ureteral orifice during embryogenesis. They are associated with ectopic insertion of the ureter with duplicated renal collecting systems in 80% of cases. Ureteroceles are most commonly detected during work-up of recurrent UTI in the pediatric population and may be associated with obstruction, urinary stasis, vesicoureteral reflux (VUR), and increased risk of stone formation [43]. On excretory phase imaging of CT urography, ureteroceles manifest as the classic “spring onion” or “cobra head” sign (Fig. 11), where the ureterocele fills with contrast surrounded by a thin radiolucent halo representing the ureterocele wall distinct from contrast within the bladder [44]. The presence of a thicker, ill-defined lucent halo or filling defect within the apparent ureterocele should raise suspicion for the so-called “pseudo-ureterocele,” which is a mimic caused by a ureterovesicular junction (UVJ) mass or calculus causing an incomplete obstruction [45].

Ureteral duplication

Ureteral duplication, also called renal duplication, is the most common congenital urogenital abnormality occurring in up to 0.5% of the population and may incidentally be encountered on CT urography. Ureteral duplication is subdivided into partial and complete. In partial, separate upper and lower pole ureters fuse at some variable distance proximal to the UVJ [2]. While partial duplication is generally considered a normal variant, it can be associated with ureteroureteral reflux, resulting in urinary stasis and may pose increased risk of UTI [46].

In complete duplication, two ureteral buds give rise to entirely separate upper and lower ureters that do not fuse (Fig. 12). The upper pole ureter has an ectopic insertion, inferior and medial to the orthotopic lower ureteral insertion, an observation referred to as the Weigert–Meyer rule [47]. Note that ectopic here means insertion in a location other than where a normal non-duplicated ureter would insert, while some papers reserve the term ectopic insertion to specifically refer to insertion outside the bladder trigone, which is of greater clinical consequence. There is a higher association of concurrent ureterocele at the upper pole insertion, as well as higher rates of VUR and obstruction [2]. The upper pole may insert on structures along the so-called “ectopic pathway,” which varies between females and males. In females, this includes the bladder, urethra, vagina, cervix, uterus, or salpinges. Insertion below the external urethral sphincter or in the reproductive organs will result in urinary incontinence. In males, possible insertions includes the bladder, prostatic urethra, seminal vesicles, vas deferens, or ejaculatory ducts in the prostate—all of which are located above the external urethral sphincter, and typically present with UTIs (Fig. 13) [2, 47].

Crossed fused renal ectopia

Crossed fused renal ectopia (CFRE) is the second most common renal fusion abnormality after horseshoe kidney that may be incidentally discovered on CT urography. CFRE is typically discovered in the asymptomatic patient, although it can present with flank pain or palpable mass [48]. It is associated with increased risk of nephrolithiasis, obstruction and hydrocephalus, VUR, and UTI [48, 49]. CFRE is a congenital abnormality in which one kidney fuses to the contralateral kidney before ascending on the contralateral side [50]. Typically, the upper pole of the crossed ectopic kidney fuses with the lower pole of the other kidney. The result is a single-fused kidney with two ureters. The fused kidney will often have aberrant arterial anatomy [48]. On non-contrast and nephrographic phases of CT urography, a single-fused kidney will be seen with two ureters. Excretory phase imaging better delineates the contrast-opacified ureter of the ectopic kidney crossing midline before inserting on the bladder at the contralateral UVJ (Fig. 14).

Chronic inflammatory conditions

Ureteritis cystica

Ureteritis cystica is a benign condition in which multiple subepithelial cysts are present in the wall of the ureter. The etiology remains unclear, although it is commonly thought to be due to indolent changes from chronic inflammation as it is often associated with stone disease and prior ureteral instrumentation. While this finding is difficult to observe on nephrographic phase images, on excretory phase it is seen as multiple punctate filling defects in the urinary tract (Fig. 15). It is important to be aware of this benign condition and to not confuse it with multifocal urothelial cancer [51].

Ureteral pseudodiverticulosis

Ureteral pseudodiverticulosis is a rare incidental finding typically discovered on CT urography during the work-up of other urinary tract disorders. It is seen on excretory phase imaging as multiple less than 5 mm outpouchings from the ureters (Fig. 16). Although this entity is thought to be related to chronic inflammation, unlike ureteritis cystica, this entity is strongly associated with malignancy within the urinary tract, with one case series reporting up to 50% of cases demonstrating coexisting urothelial malignancy [52].

Conclusion

CT urography has become the primary imaging modality in evaluating hematuria and is commonly used in staging and surveillance of urinary tract malignancies. It also has value for evaluating renal papillary abnormalities, perinephric fluid collections, CT radiolucent stones, congenital abnormalities, and chronic inflammatory conditions. The non-contrast, nephrographic, and excretory phases of CT urography provide powerful diagnostic ability when combined, but also have the potential to add substantial patient radiation dose. The use of AEC, IR algorithms, split-bolus dosing in patients under age 40, and tolerating higher noise in certain phases are a few techniques reviewed here to mitigate the issue of increased radiation dose. With these techniques, it is possible to perform high-quality, low-dose CT urography.

References

1. Van Der Molen AJ, Cowan NC, Mueller-Lisse UG, et al. (2008) CT urography: definition, indications and techniques. A guideline for clinical practice. Eur Radiol 18:4–17. 10.1007/s00330-007-0792-x [PubMed: 17973110]
2. Potenta SE, D'Agostino R, Sternberg KM, et al. (2015) CT Urography for Evaluation of the Ureter. RadioGraphics 35:709–726. 10.1148/rg.2015140209 [PubMed: 25815907]
3. Shen L, Raman SS, Beland MD, et al. (2015) ACR Appropriateness Criteria ® Hematuria. In: Am. Coll. Radiol https://acsearch.acr.org/docs/69490/Narrative/. Accessed 6 Feb 2019
4. van der Pol CB, Sahni VA, Eberhardt SC, et al. (2017) ACR Appropriateness Criteria ® Pretreatment Staging of Muscle-Invasive Bladder Cancer. In: Am. Coll. Radiol, https://acsearch.acr.org/docs/69370/Narrative/. Accessed 6 Feb 2019
5. Leyendecker JR, Clingan MJ, Eberhardt SC, et al. (2014) ACR Appropriateness Criteria ® Post-Treatment Surveillance of Bladder Cancer. In: Am. Coll. Radiol, https://acsearch.acr.org/docs/69364/Narrative/. Accessed 6 Feb 2019
6. Moreno CC, Beland MD, Goldfarb S, et al. (2015) ACR Appropriateness Criteria ® Acute Onset Flank Pain-Suspicion of Stone Disease. https://acsearch.acr.org/docs/69362/Narrative/. Accessed 27 Feb 2019
7. Silverman SG, Leyendecker JR, Amis ES (2009) What Is the Current Role of CT Urography and MR Urography in the Evaluation of the Urinary Tract? Radiology 250:309–323. 10.1148/radiol.2502080534 [PubMed: 19188307]
8. ICRP (1991) 1990 Recommendations of the International Commission on Radiological Protection. Ann ICRP 21:1–201
9. Prakash P, Kalra MK, Kambadakone AK, et al. (2010) Reducing Abdominal CT Radiation Dose With Adaptive Statistical Iterative Reconstruction Technique. Invest Radiol 45:202–210. 10.1097/RLI.ob013e3181dzfeec [PubMed: 20177389]
10. Sagara Y, Hara AK, Pavlicek W, et al. (2010) Abdominal CT: comparison of low-dose CT with adaptive statistical iterative reconstruction and routine-dose CT with filtered back projection in 53 patients. AJR Am J Roentgenol 195:713–719. 10.2214/AJR.09.2989 [PubMed: 20729451]
11. van der Molen AJ, Miclea RL, Geleijns J, Joemai RMS (2015) A Survey of Radiation Doses in CT Urography Before and After Implementation of Iterative Reconstruction. AJR Am J Roentgenol 205:572–577. 10.2214/AJR.14.13862 [PubMed: 26295643]
12. McCollough CH, Bruesewitz MR, Kofler JM (2006) CT dose reduction and dose management tools: overview of available options. Radiographics 26:503–512. 10.1148/rg.262055138 [PubMed: 16549613]
13. Hack K, Pinto PA, Gollub MJ (2012) Targeted Delayed Scanning at CT Urography: A Worthwhile Use of Radiation? Radiology 265:143–150. 10.1148/radiol.12110548 [PubMed: 22855323]
14. Lisanti CJ, Toffoli TJ, Stringer MT, et al. (2014) CT Evaluation of the Upper Urinary Tract in Adults Younger Than 50 Years With Asymptomatic Microscopic Hematuria: Is IV Contrast Enhancement Needed? Am J Roentgenol 203:615–619. 10.2214/AJR.13.11891 [PubMed: 25148165]
15. Lokken RP, Sadow CA, Silverman SG (2012) Diagnostic Yield of CT Urography in the Evaluation of Young Adults With Hematuria. Am J Roentgenol 198:609–615. 10.2214/AJR.11.7296 [PubMed: 22358000]
16. Mace LR, Galloway TL, Ma A, et al. (2017) Diagnostic yield of CT urography in the evaluation of hematuria in young patients in a military population. Abdom Radiol 42:1906–1910. 10.1007/s00261-017-1084-9
17. Dahlman P, van der Molen AJ, Magnusson M, Magnusson A (2012) How much dose can be saved in three-phase CT urography? A combination of normal-dose corticomedullary phase with low-dose unenhanced and excretory phases. AJR Am J Roentgenol 199:852–860. 10.2214/AJR.11.7209 [PubMed: 22997378]
18. Yu L, Bruesewitz MR, Thomas KB, et al. (2011) Optimal tube potential for radiation dose reduction in pediatric CT: principles, clinical implementations, and pitfalls. Radiographics 31:835–848. 10.1148/rg.313105079 [PubMed: 21571660]

19. Lira D, Padole A, Kalra MK, Singh S (2015) Tube Potential and CT Radiation Dose Optimization. Am J Roentgenol 204:W4–W10. 10.2214/AJR.14.13281 [PubMed: 25539272]
20. Yu L, Li H, Fletcher JG, McCollough CH (2010) Automatic selection of tube potential for radiation dose reduction in CT: a general strategy. Med Phys 37:234–243. 10.1118/1.3264614 [PubMed: 20175486]
21. Yanaga Y, Awai K, Funama Y, et al. (2009) Low-dose MDCT urography: feasibility study of low-tube-voltage technique and adaptive noise reduction filter. AJR Am J Roentgenol 193:W220–W229. 10.2214/AJR.08.1710 [PubMed: 19696263]
22. Kaza RK, Platt JF, Cohan RH, et al. (2012) Dual-Energy CT with Single- and Dual-Source Scanners: Current Applications in Evaluating the Genitourinary Tract. RadioGraphics 32:353–369. 10.1148/rg.322115065 [PubMed: 22411937]
23. Takahashi N, Vrtiska TJ, Kawashima A, et al. (2010) Detectability of Urinary Stones on Virtual Nonenhanced Images Generated at Pyelographic-Phase Dual-Energy CT. Radiology 256:184–190. 10.1148/radiol.10091411 [PubMed: 20574095]
24. Chen C-Y, Tsai T-H, Jaw T-S, et al. (2016) Diagnostic Performance of Split-Bolus Portal Venous Phase Dual-Energy CT Urography in Patients With Hematuria. Am J Roentgenol 206:1013–1022. 10.2214/AJR.15.15112 [PubMed: 26934212]
25. Humphrey PA, Moch H, Cubilla AL, et al. (2016) The 2016 WHO Classification of Tumours of the Urinary System and Male Genital Organs-Part B: Prostate and Bladder Tumours. Eur Urol 70:106–119. 10.1016/j.eururo.2016.02.028 [PubMed: 26996659]
26. Rouprêt M, Babjuk M, Compérat E, et al. (2018) European Association of Urology Guidelines on Upper Urinary Tract Urothelial Carcinoma: 2017 Update. Eur Urol 73:111–122. 10.1016/j.eururo.2017.07.036 [PubMed: 28867446]
27. Cosentino M, Palou J, Gaya JM, et al. (2013) Upper urinary tract urothelial cell carcinoma: location as a predictive factor for concomitant bladder carcinoma. World J Urol 31:141–145. 10.1007/s00345-012-0877-2
28. Babjuk M, Böhle A, Burger M, et al. (2017) EAU Guidelines on Non-Muscle-invasive Urothelial Carcinoma of the Bladder: Update 2016. Eur Urol 71:447–461. 10.1016/j.eururo.2016.05.041 [PubMed: 27324428]
29. Rouprêt M, Babjuk M, Compérat E, et al. (2015) European Association of Urology Guidelines on Upper Urinary Tract Urothelial Cell Carcinoma: 2015 Update. Eur Urol 68:868–879. 10.1016/j.eururo.2015.06.044 [PubMed: 26188393]
30. Holmäng S, Lele SM, Johansson SL (2007) Squamous cell carcinoma of the renal pelvis and ureter: incidence, symptoms, treatment and outcome. J Urol 178:51–56. 10.1016/j.juro.2007.03.033 [PubMed: 17574059]
31. Chao CH, Fong TC, Hughes-Cassidy F, Aganovic L (2012) Ureteral Intussusception. J Comput Assist Tomogr 36:261–264. 10.1097/RCT.0b013e31824677a5 [PubMed: 22446371]
32. Gambaro G, Feltrin GP, Lupo A, et al. (2006) Medullary sponge kidney (Lenarduzzi–Cacchi–Ricci disease): A Padua Medical School discovery in the 1930s. Kidney Int 69:663–670. 10.1038/SJ.KI.5000035 [PubMed: 16395272]
33. Maw AM, Megibow AJ, Grasso M, Goldfarb DS (2007) Diagnosis of Medullary Sponge Kidney by Computed Tomographic Urography. Am J Kidney Dis 50:146–150. 10.1053/J.AJKD.2007.03.020 [PubMed: 17591535]
34. Jung DC, Kim SH, Il Jung S, et al. (2006) Renal Papillary Necrosis: Review and Comparison of Findings at Multi-Detector Row CT and Intravenous Urography. RadioGraphics 26:1827–1836. 10.1148/rg.266065039 [PubMed: 17102053]
35. Hartman MS (2006) The Golf Ball–on-Tee Sign. Radiology 239:297–298. 10.1148/radiol.2391031947 [PubMed: 16567491]
36. Alabousi A, Patlas MN, Menias CO, et al. (2017) Multi-modality imaging of the leaking ureter: why does detection of traumatic and iatrogenic ureteral injuries remain a challenge? Emerg Radiol 24:417–422. 10.1007/s10140-017-1507-5 [PubMed: 28451770]
37. Gershman B, Kulkarni N, Sahani DV, Eisner BH (2011) Causes of renal forniceal rupture. BJU Int 108:1909–1911. 10.1111/j.1464-410X.2011.10164.x [PubMed: 21736690]

38. Sandhu C, Anson K, Patel U (2003) Urinary Tract Stones—Part I: Role of Radiological Imaging in Diagnosis and Treatment Planning. Clin Radiol 58:415–421. 10.1016/S0009-9260(03)00103-X [PubMed: 12788310]
39. Sundaram CP, Saltzman B (1999) Urolithiasis Associated with Protease Inhibitors. J Endourol 13:309–312 [PubMed: 10405912]
40. Nadler RB, Rubenstein JN, Eggener SE, et al. (2003) The Etiology of Urolithiasis in HIV Infected Patients. J Urol 169:475–477. 10.1016/S0022-5347(05)63936-5 [PubMed: 12544290]
41. Bani-Hani AH, Segura JW, Leroy AJ (2005) Urinary matrix calculi: our experience at a single institution. J Urol 173:120–123. 10.1097/01.ju.0000145868.18824.25 [PubMed: 15592051]
42. Stoller ML, Gupta M, Bolton D, Irby PB (1994) Clinical Correlates of the Gross, Radiographic, and Histologic Features of Urinary Matrix Calculi. J Endourol 8:335–340. 10.1089/end.1994.8.335 [PubMed: 7858618]
43. Coplen DE, Duckett JW (1995) The Modern Approach to Ureteroceles. J Urol 153:166–171. 10.1097/00005392-199501000-00068 [PubMed: 7966763]
44. Dyer RB, Chen MY, Zagoria RJ (2004) Classic Signs in Uroradiology. RadioGraphics 24:S247–S280. 10.1148/rg.24si045509 [PubMed: 15486245]
45. Chavhan GB (2002) The Cobra Head Sign. Radiology 225:781–782. 10.1148/radiol.2253011206 [PubMed: 12461261]
46. Fernbach SK, Feinstein KA, Spencer K, Lindstrom CA (1997) Ureteral duplication and its complications. RadioGraphics 17:109–127. 10.1148/radiographics.17.L9017803 [PubMed: 9017803]
47. Didier RA, Chow JS, Kwatra NS, et al. (2017) The duplicated collecting system of the urinary tract: embryology, imaging appearances and clinical considerations. Pediatr Radiol 47:1526–1538. 10.1007/s00247-017-3904-z [PubMed: 29043421]
48. Türkvatan A, Olçer T, Cumhur T (2009) Multidetector CT urography of renal fusion anomalies. Diagn Interv Radiol 15:127–134 [PubMed: 19517383]
49. Guarino N, Tadini B, Camardi P, et al. (2004) The incidence of associated urological abnormalities in children with renal ectopia. J Urol 172:1757–9; discussion 1759 [PubMed: 15371807]
50. Friedland GW, de Vries P (1975) Renal ectopia and fusion. Embryologic Basis. Urology 5:698–706 [PubMed: 1129903]
51. Menéndez V, Sala X, Alvarez-Vijande R, et al. (1997) Cystic pyeloureteritis: Review of 34 cases. Radiologic aspects and differential diagnosis. Urology 50:31–37. 10.1016/S0090-4295(97)00205-7 [PubMed: 9218015]
52. Wasserman NF, Zhang G, Posalaky IP, Reddy PK (1991) Ureteral pseudodiverticula: frequent association with uroepithelial malignancy. AJR Am J Roentgenol 157:69–72. 10.2214/ajr.157.1.1904678 [PubMed: 1904678]

Fig. 1.

Normal appearance of the three phases of CT urography is provided for reference. **a** Non-contrast axial image through the kidneys shows no renal calcifications or high attenuation masses. **b** Nephrographic phase axial image through the kidneys show symmetric parenchymal enhancement without parenchymal mass. **c** Excretory phase axial image through the kidneys shows symmetric excreted contrast in bilateral renal pelvises. Symmetric contrast opacification of the ureters (arrows) to the level of the bladder, as shown on **d** the coronal reformatted excretory phase image and **e** the excretory phase axial image at the level of the ureteral insertion to the bladder

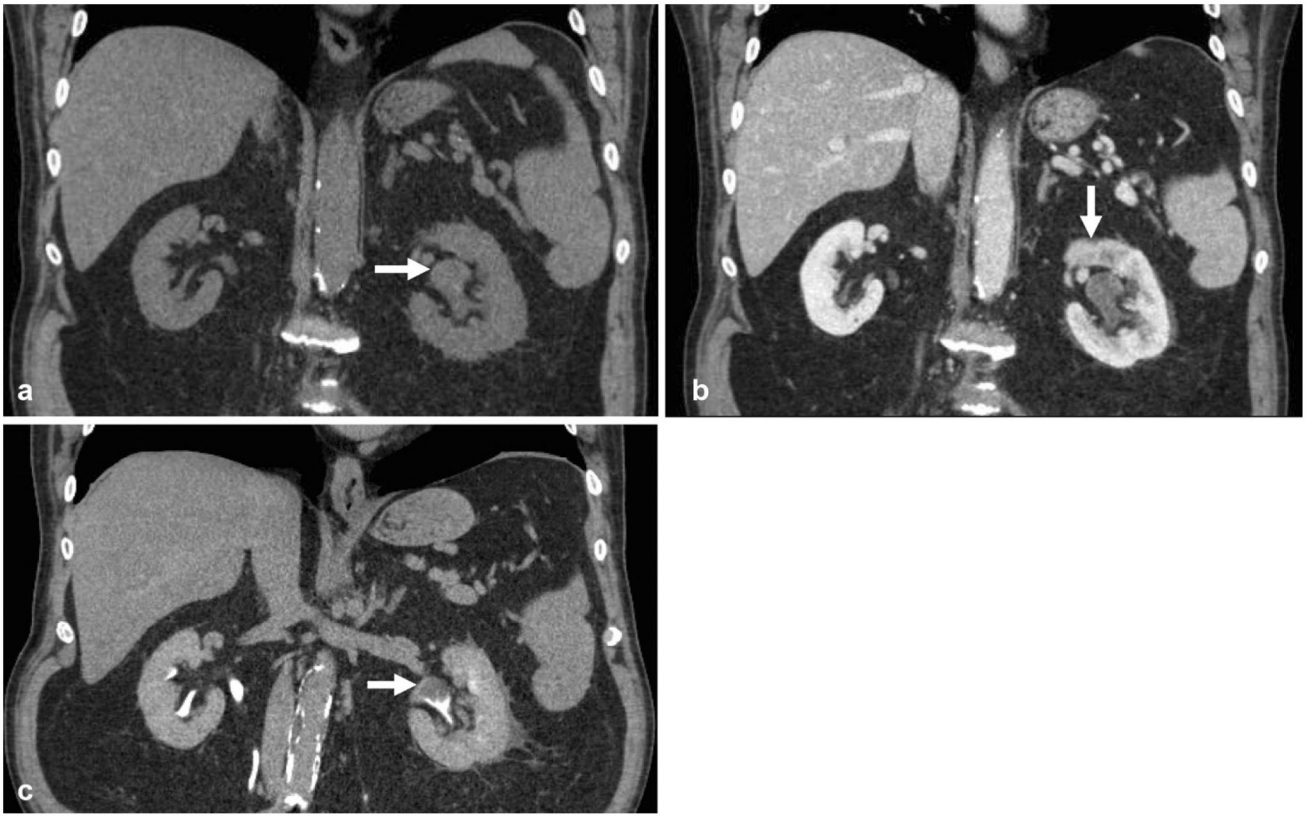

Fig. 2.

CT urogram was obtained in this 63-year-old male for evaluation of gross hematuria. **a** Non-contrast coronal reformatted image shows mild left pelviectasis (arrow). **b** Nephrographic phase coronal reformatted image shows subtle heterogeneous enhancement in the left renal pelvis (arrow) and delayed left nephrogram relative to the right. **c** Excretory phase coronal reformatted image shows a clear filling defect within the renal pelvis (arrow), which was later confirmed as urothelial carcinoma

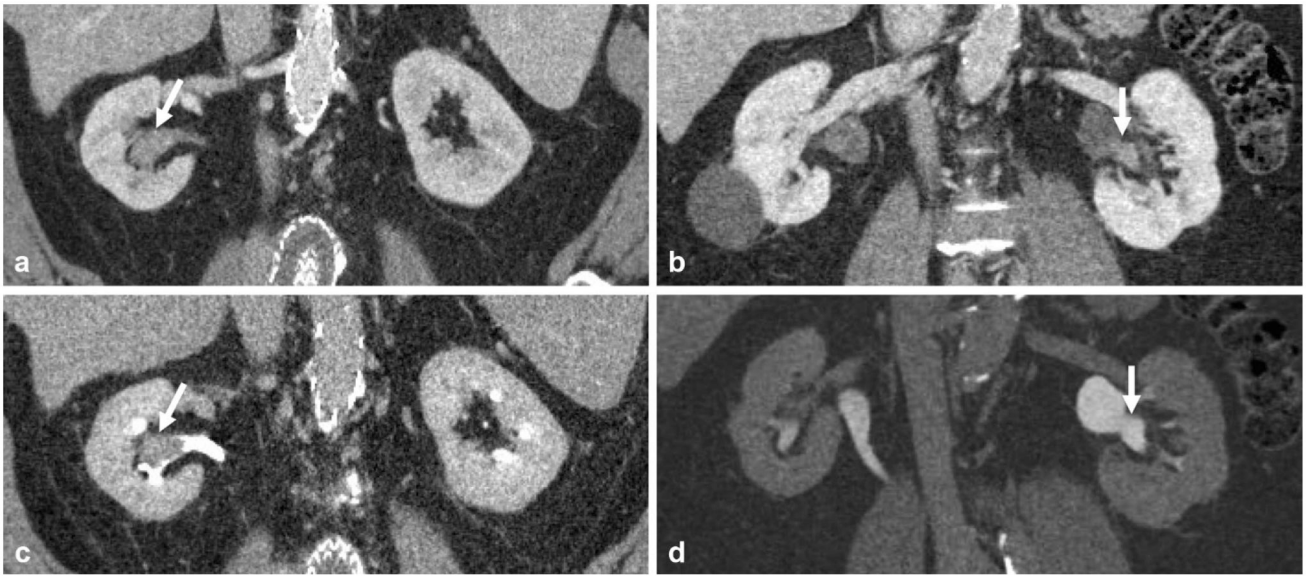

Fig. 3.

Companion cases of two different adult patients presenting with microscopic hematuria demonstrating the utility of the excretory phase in delineating early excretion on nephrographic phase versus enhancing mass in the renal pelvis. **a** Nephrographic phase coronal reformatted image demonstrates high density in the renal pelvis (arrow), which could be early excretion or enhancing mass. **b** Excretory phase coronal reformatted image demonstrates this corresponds to a filling defect (arrow), and was in fact an enhancing soft-tissue mass, later confirmed to be urothelial carcinoma. **c** Nephrographic phase coronal reformatted image in a different patient demonstrates similar high density (arrow) in the renal pelvis; however. **d** excretory phase shows this area opacifies with contrast (arrow) and confirms this as early excretion of contrast on the nephrographic phase

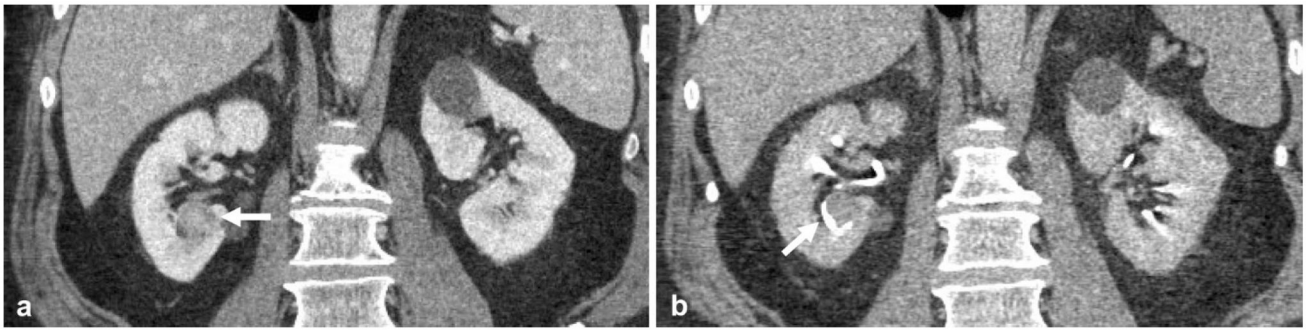

Fig. 4.

A 60-year-old male with microhematuria. **a** Nephrographic phase coronal reformatted image demonstrates a lower pole mass (arrow). It is difficult to determine whether the mass arises from renal parenchyma, such as a renal cell carcinoma (RCC), or from the renal collecting system, such as a urothelial carcinoma. **b** Excretory phase coronal reformatted image better delineates the anatomy and shows the lower pole calyx (arrow) is displaced by the mass, confirming that the mass does not arise from the calyx and thus is most likely a renal cell carcinoma. This was later confirmed to be a papillary RCC at pathology

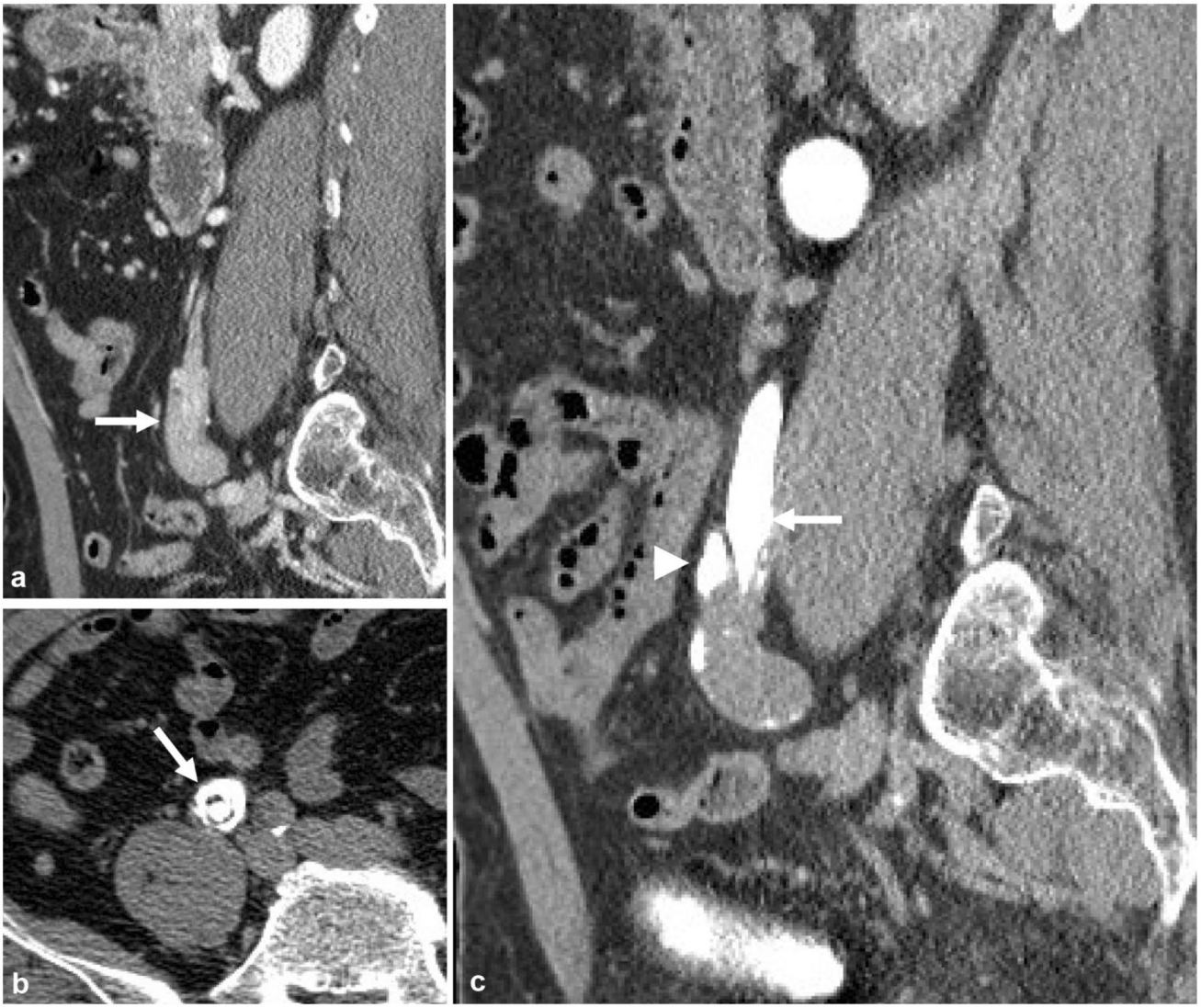

Fig. 5.

A 65-year-old male with microhematuria and flank pain. **a** Nephrographic phase sagittal reformatted image demonstrates bulbous appearing mass at the distal right ureter (arrow). **b** Excretory phase axial image better demonstrates contrast circumferentially in a “target sign” appearance suggestive of ureteroureteral intussusception (arrow), which was due to a urothelial carcinoma as a lead point. **c** Excretory phase sagittal reformatted image demonstrates tapering of the distal ureter, or the intussusceptum (arrow), with contrast seen peripherally, also called the intussuscipiens (arrowhead)

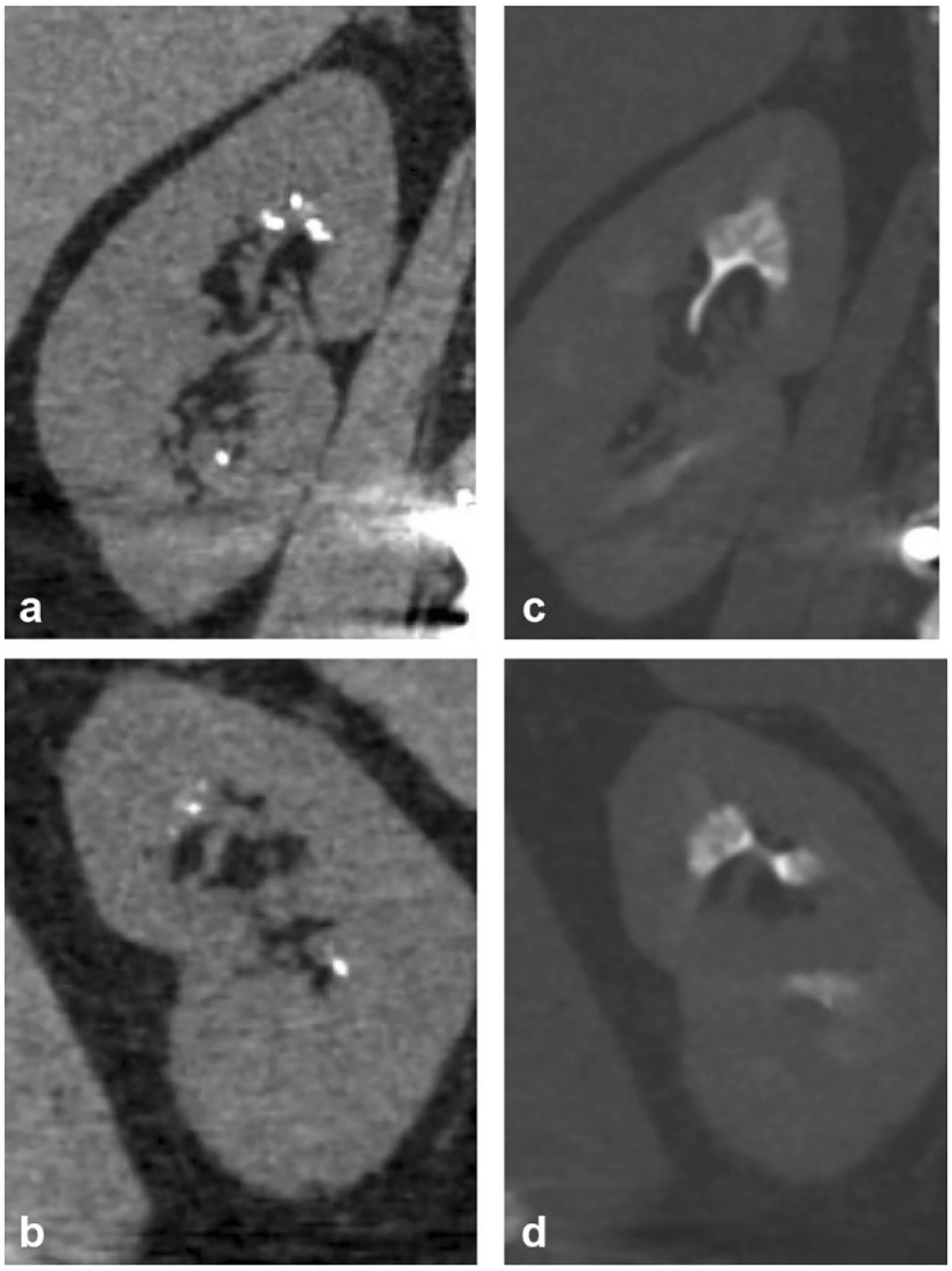

Fig. 6.

A 63-year-old male undergoing work-up for renal insufficiency. Non-contrast coronal reformatted images of the left **(a)** and right **(b)** kidneys demonstrate medullary calcifications in bilateral kidneys that may easily be mistaken for small renal calculi. Excretory phase coronal reformatted images in bone windows of the left **(c)** and right **(d)** kidneys demonstrate the characteristic “paintbrush appearance” of medullary sponge kidney, presumably from contrast filling-dilated medullary collecting ducts

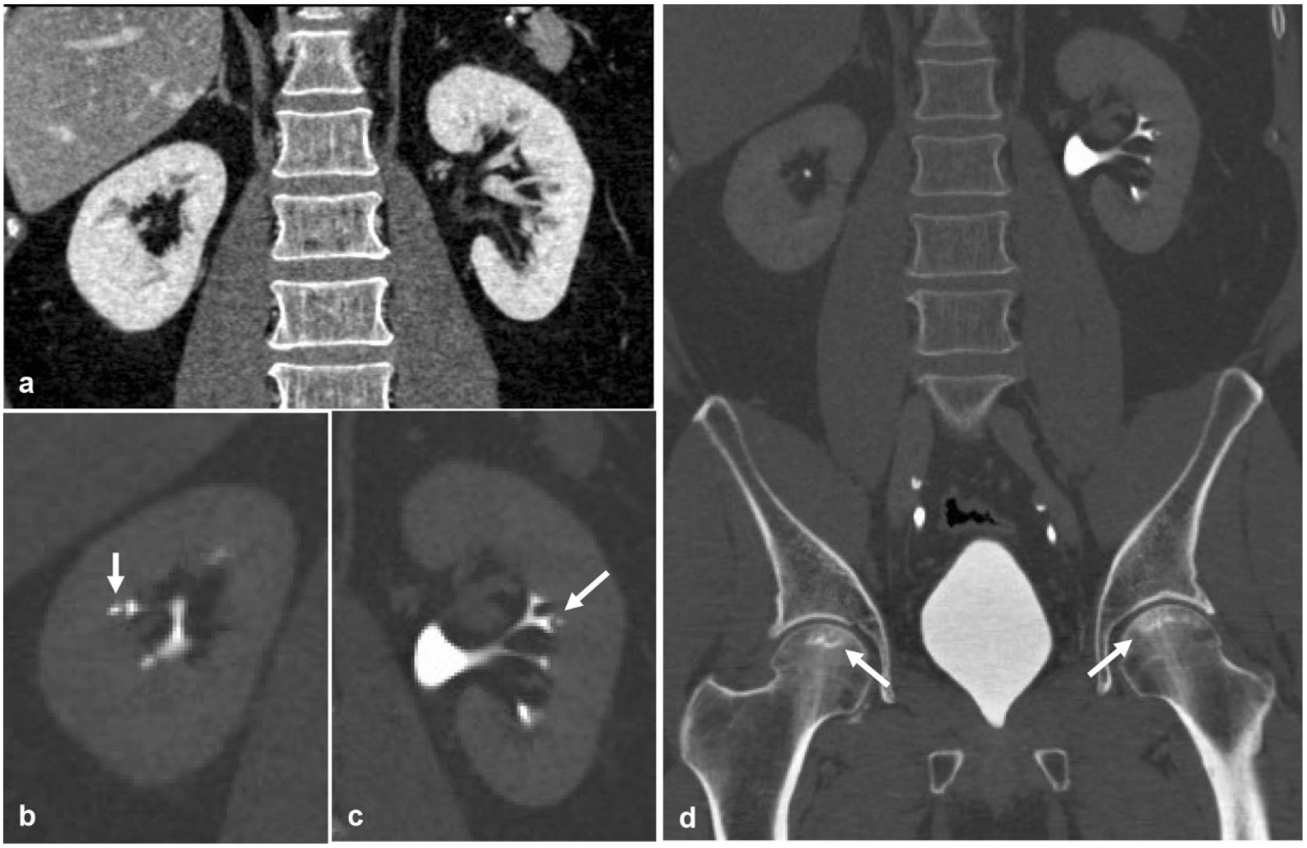

Fig. 7.

A 29-year-old male with sickle cell disease presents with bilateral flank pain. **a** Nephrographic phase coronal reformatted image of the kidney demonstrates an otherwise normal appearing symmetric nephrogram. Excretory phase coronal reformatted images in bone windows of the **b** right and **c** left kidneys demonstrate the classic “golf ball on tee” sign (arrow) of renal papillary necrosis. **d** Bilateral femoral head osteonecrosis (arrows) is also seen, which in the absence of the given history would help solidify sickle cell disease as the etiology behind this patient’s renal papillary necrosis

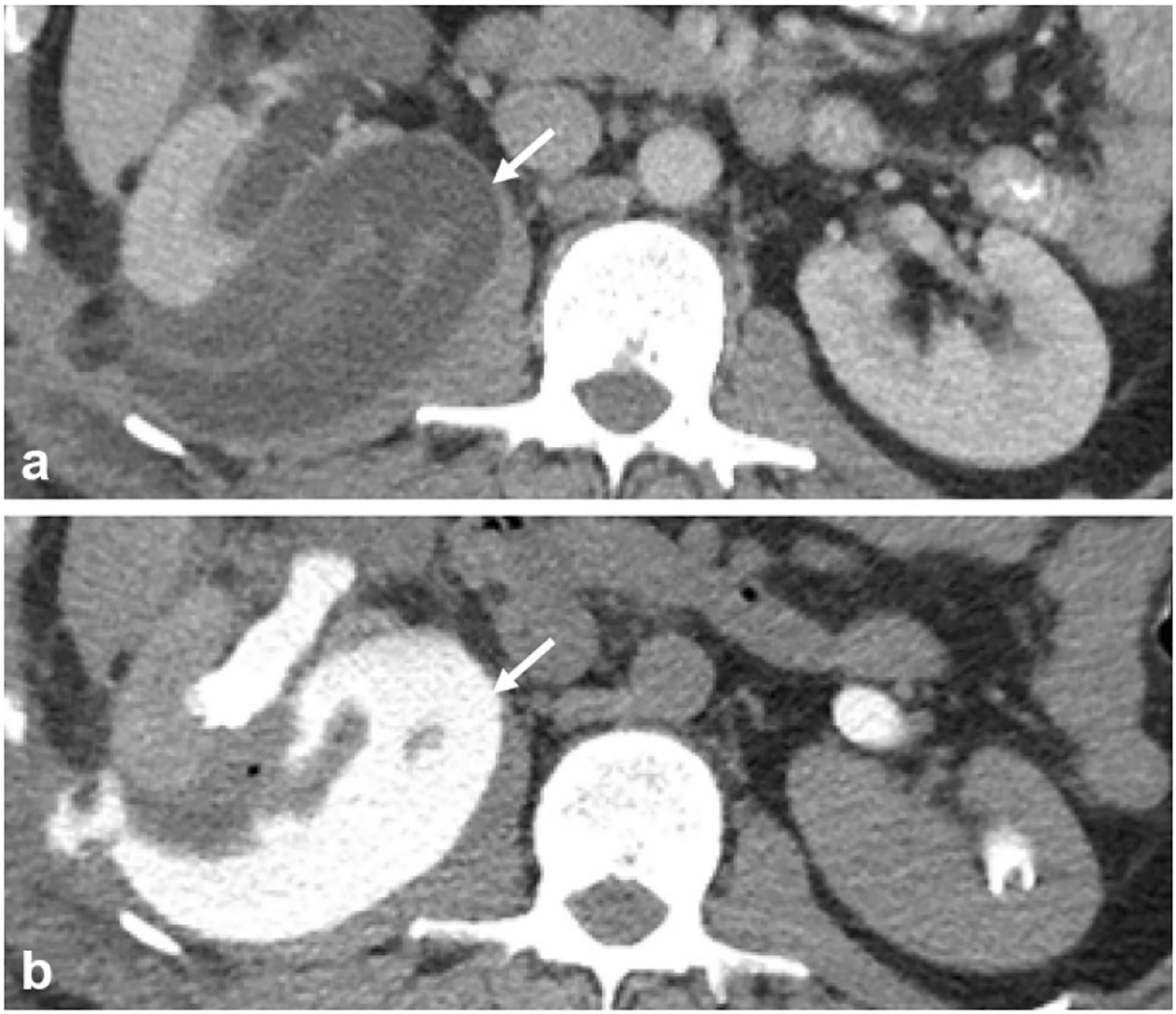

Fig. 8.

A 32-year-old status post right-sided partial nephrectomy. **a** Nephrographic phase axial image shows a complex fluid collection (arrow) adjacent to the recently operated on right kidney. **b** Excretory phase axial image demonstrates contrast opacification of the fluid collection (arrow) compatible with a post-operative urinoma

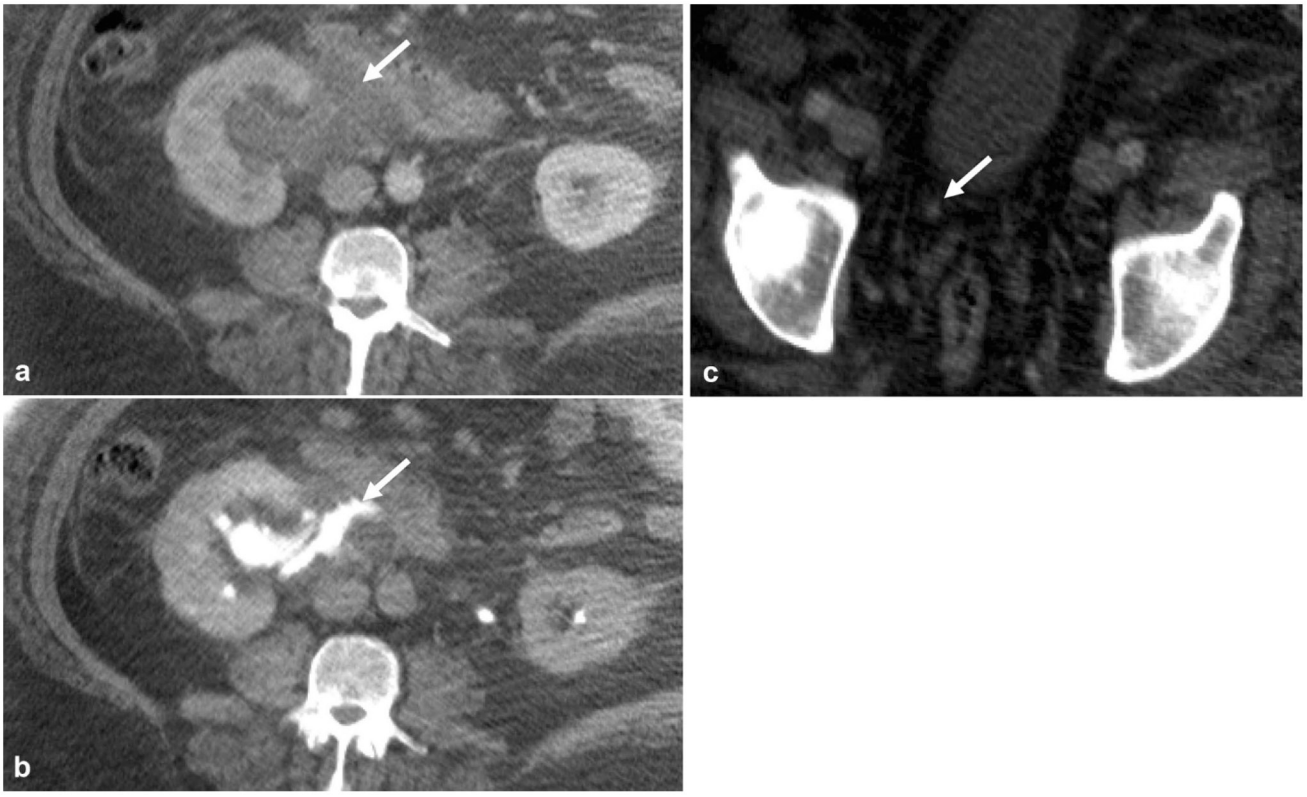

Fig. 9.

A 50-year-old male with right flank pain that acutely improved before CT exam. **a** Nephrographic phase axial image shows a right peripelvic fluid collection. **b** Excretory phase axial image shows contrast extending into the fluid collection from the renal pelvis compatible with a urinoma from forniceal rupture, which in this case was confirmed to be secondary to a **c** 2-mm obstructing distal ureteral stone (arrow)

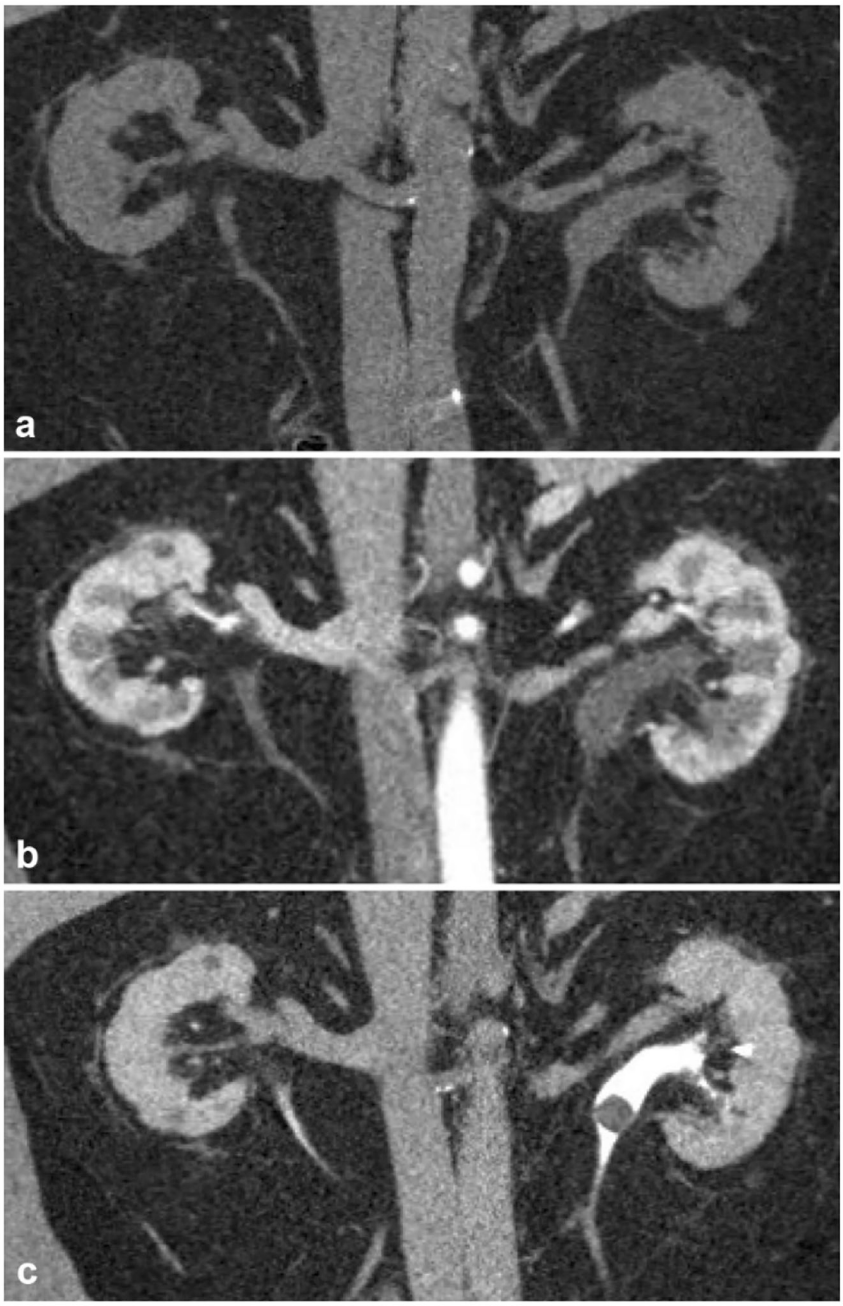

Fig. 10.

A 53-year-old patient with renal colic. **a** Non-contrast coronal reformatted image demonstrates mild left hydroureter without evidence of a radiopaque ureteral calculus. **b** Nephrographic phase coronal reformatted image demonstrates symmetric enhancement without an apparent cause for the left-sided hydroureter. **c** Excretory phase coronal reformatted image demonstrates a rounded filling defect in the proximal left ureter, which was later confirmed at pathology to be a matrix stone

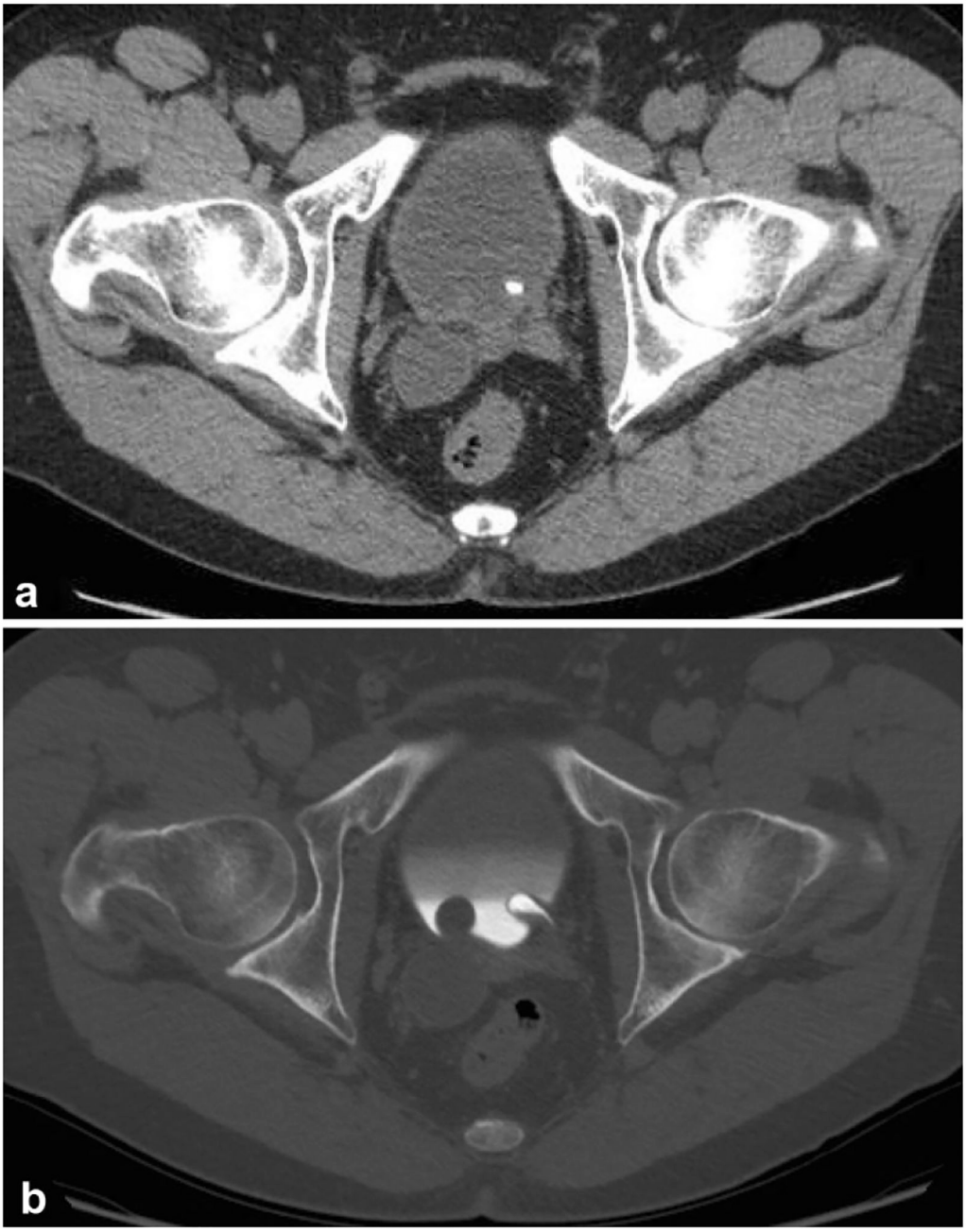

Fig. 11.

A 47-year-old male with incidental finding of right-sided hydroureter on imaging for work-up of an unrelated issue. **a** Non-contrast axial image of the pelvis demonstrates right distal hydroureter. There is also a high density in the bladder in the region of the left ureterovesicular junction (UVJ). **b** Excretory phase axial image on bone windows demonstrates bilateral ureteroceles, non-opacified on the right due to impaired excretion by the right kidney. The classic “spring onion” sign is best demonstrated on the left where the ureterocele is opacified with contrast. The left UVJ calculus seen on the non-contrast image

is shown to be within the left ureterocele. The ureterocele on the right is likely the cause of this patient's right-sided hydroureter

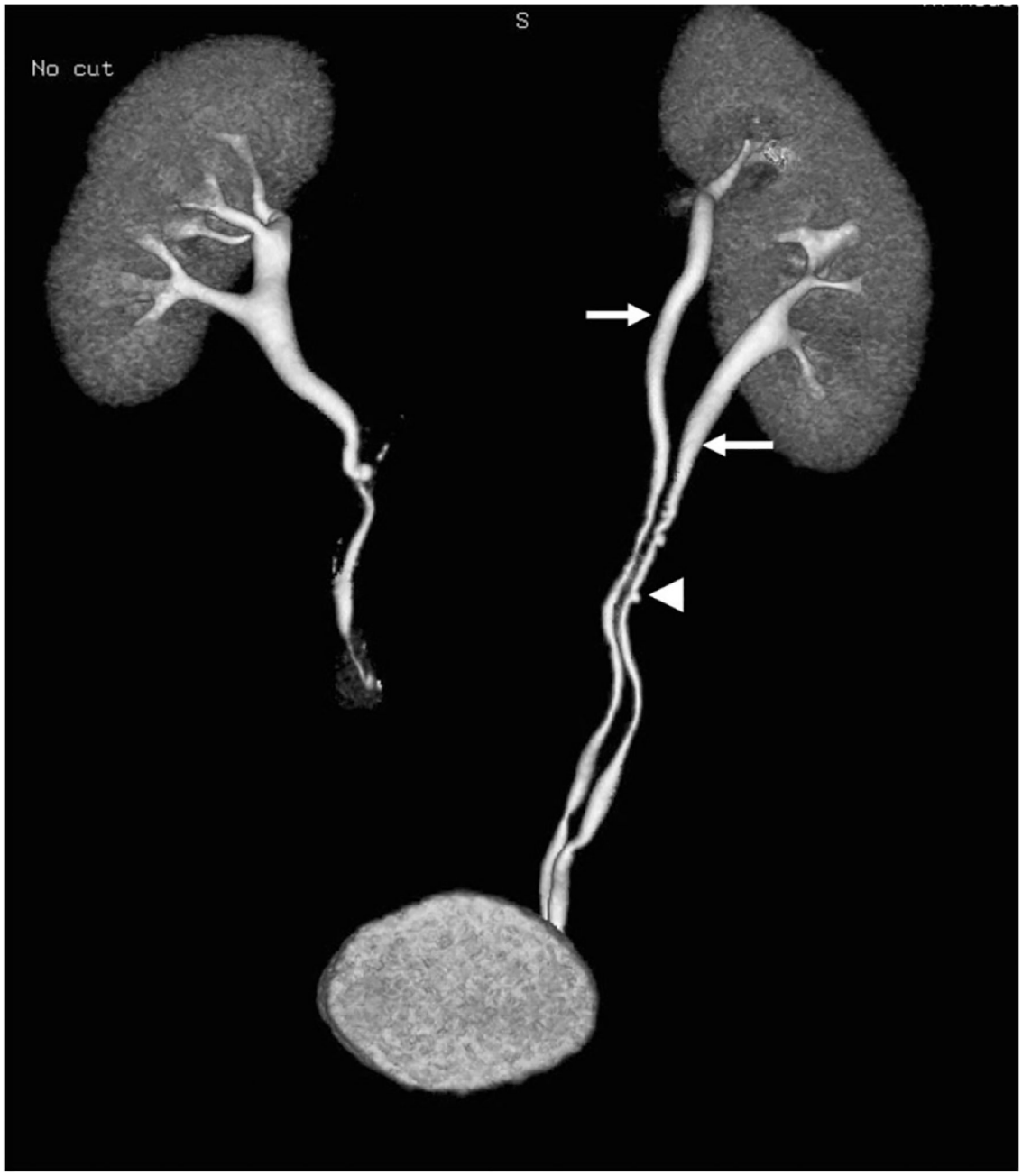

Fig. 12.

A 66-year-old patient undergoing work-up of microscopic hematuria. An excretory phase 3D reconstruction demonstrates a complete ureteral duplication with completely separate upper and lower ureters (arrows) along their respective course, both of which insert on the bladder. There is incidentally noted concurrent ureteral pseudodiverticulosis (arrowhead)

Fig. 13.

A 39-year-old male undergoing further work-up after incidental finding of bilateral hydroureteronephrosis on imaging performed for unrelated symptoms. **a** Excretory phase coronal image demonstrates bilateral complete ureteral duplication with hydronephrosis of bilateral upper moieties (arrows) with insertion of the upper pole ureters onto the prostatic urethra (arrowhead). **b** Additional coronal reformatted image demonstrates the upper pole hydroureter (arrow) and normal lower pole ureter (arrowhead). **c** Excretory phase axial image again demonstrates ectopic insertion of the upper pole ureters onto the prostatic urethra (arrow)

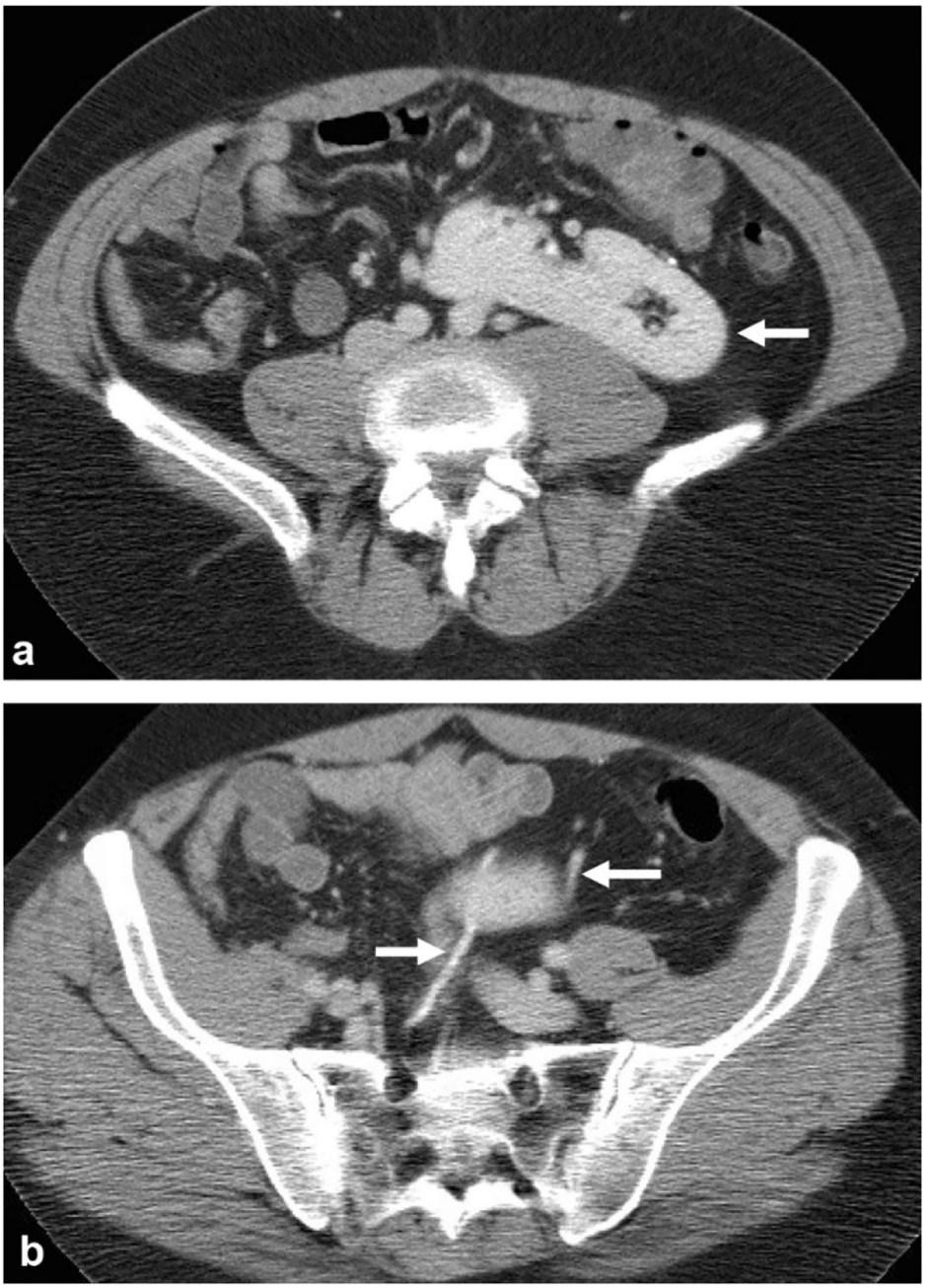

Fig. 14.

A 46-year-old female presents with abdominal pain, incidentally found to have crossed fused renal ectopia. **a** Nephrographic phase axial image at the level of the kidneys shows an ectopic right kidney fused to the left kidney (arrow) in the left upper quadrant. **b** Excretory phase axial image shows two ureters (arrow), one of which crosses midline to the right hemiabdomen before inserting on the bladder at the right UVJ

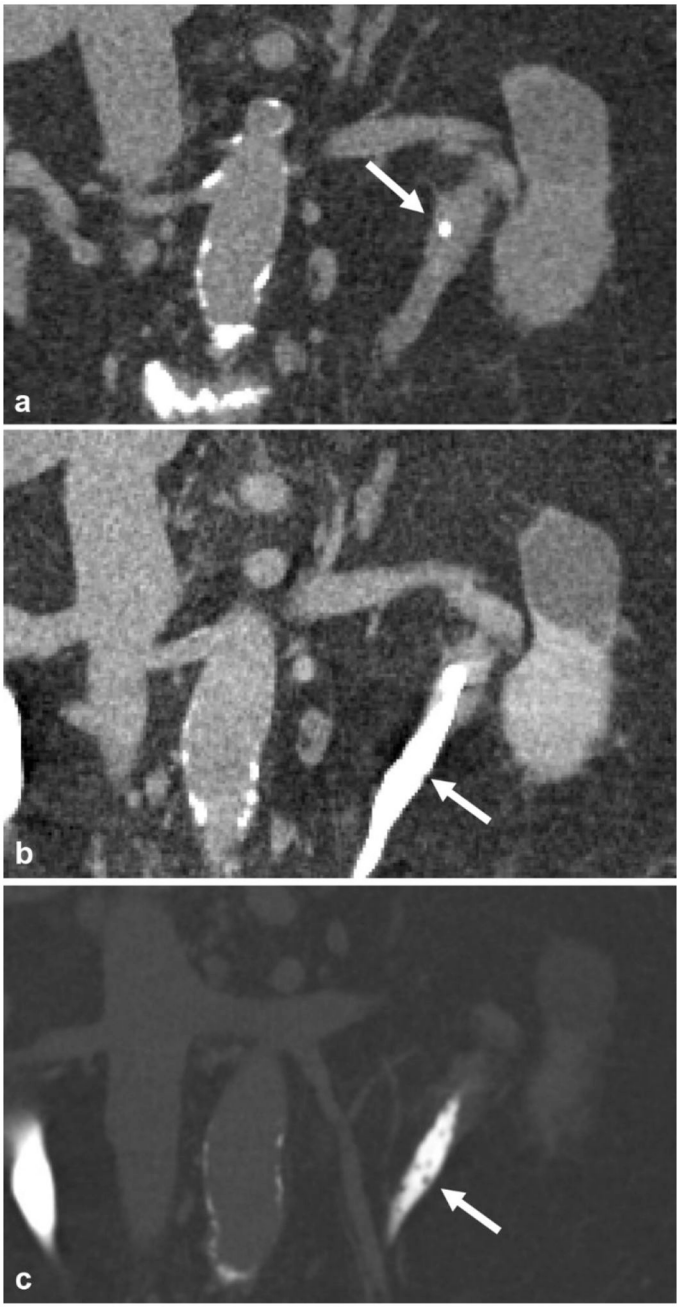

Fig. 15.

A 72-year-old female with chronic UTI. **a** Non-contrast coronal reformatted image demonstrates a ureteral stone (arrow) in the left proximal ureter. **b** Excretory phase coronal reformatted image shows very subtle indentations (arrow) in the proximal and mid ureter. **c** The same coronal reformatted image in bone windows reveals multiple uniform tiny filling defects (arrow) in the proximal and mid ureter, which represent multiple subepithelial cysts in the wall of the ureter from ureteritis cystica

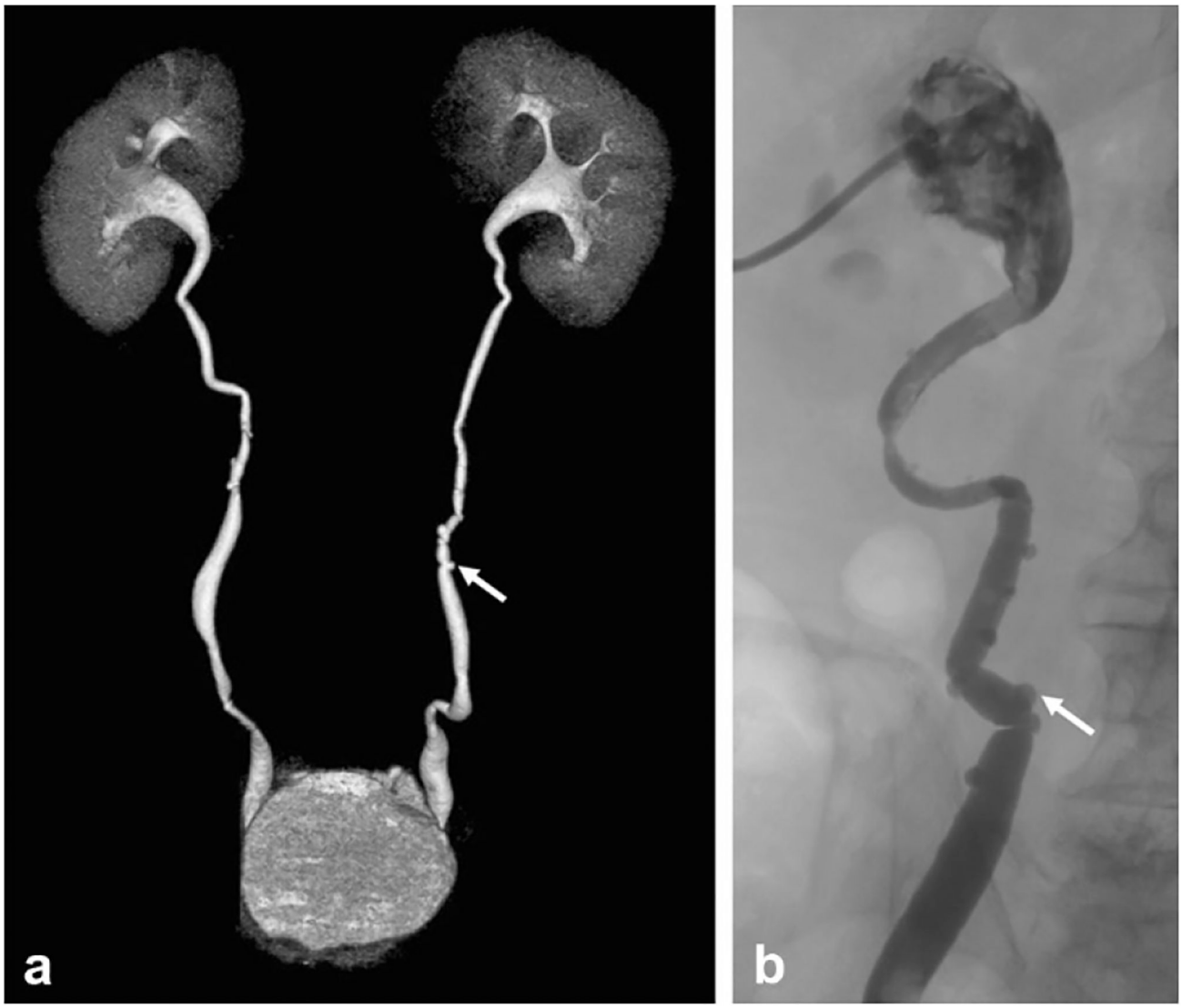

Fig. 16.

Two cases of ureteral pseudodiverticulosis in adult patients undergoing work-up of microscopic hematuria demonstrating multiple tiny, less than 5 mm, outpouchings from the ureters (arrows) on a **a** 3D reformatted image from excretory phase imaging on CT urography and on **b** antegrade pyelography

Abdom Radiol (NY). Author manuscript; available in PMC 2022 February 27.

Table 1

Summary of ACR appropriateness criteria related to CT urography

Clinical indication	Appropriateness of CT urography
Hematuria	First-line modality in patients with hematuria who do not meet 1 of 2 criteria: **1** History of associated vigorous exercise, infection, recent viral illness, or recent menstruation **2** Patients with renal parenchymal disease known to cause hematuria, such as glomerulonephritis
Staging of muscle-invasive bladder cancer	Used to evaluate for concomitant upper tract urothelial carcinoma, as well as staging of pelvic lymph nodes or more distant metastases in the abdomen
Surveillance of bladder cancer post-treatment	Generally appropriate in any patient with findings of invasive urothelial carcinoma or superficial urothelial carcinoma with risk factors. Risk factors include carcinoma in situ (CIS) on pathology, size > 3 cm, higher-grade, adjacent or remote atypia or high-grade dysplasia of the bladder mucosa, multifocal cancer, upper tract obstruction at presentation, lymphatic invasion, involvement of the prostate
Acute onset flank pain with suspicion for urolithiasis	Excretory phase imaging may be appropriate if non-contrast CT is indeterminate in distinguishing a calcific density as within the ureter versus adjacent phlebolith, while standard contrast-enhanced CT may be appropriate if a non-contrast exam does not elicit the cause of the patient's pain.

Adapted with permission from American College of Radiology (ACR) Appropriateness Criteria

Table 2

Low-dose multiphase parameters used for the CT urogram protocol in patients over 40

Phase[a]	Tube potential (kVp)	Fixed noise index	AEC[c] variable mA dose modulation range	ASiR (%)
Non-contrast[b]	120	37.0	150–750	40
Nephrographic[b]	120	32.0	150–750	30
Excretory[b]	100	37.0	150–675	40

kVp kilovoltage peak, *AEC* automatic exposure control, *mA* milliamperes, *ASiR* adaptive statistical iterative reconstruction, GE Healthcare

[a] CT urograms are performed on a 64-MDCT scanner (Lightspeed VCT, GE Healthcare)

[b] All phases are performed at 0.625-mm collimation with 2.5-mm reconstruction slice thickness

[c] AEC utilized both GE Auto mA and Smart mA